ANNALS OF GEOPHYSICS, 61, 2, SE228, 2018; doi: 10.441/ag-7711

"MULTISCALE PROCESSES TO DESCRIBE THE EASTERN SICILY SEISMIC SEQUENCES"

Marianna Siino[1], Antonino D'Alessandro[2], Giada Adelfio[1,2,*], Salvatore Scudero[2] and Marcello Chiodi[1,2]

(1) Dipartimento di Scienze Economiche, Aziendali e Statistiche, Università degli Studi di Palermo, Palermo, Italy
(2) Istituto Nazionale di Geofisica e Vulcanologia, Centro Nazionale Terremoti, Rome, Italy

Article history
Receveid November 26, 2016; accepted September 5, 2017.
Subject classification:
Earthquakes; Point process; Hybrid of Gibbs process; Residual G-function; Spatial raw residuals

ABSTRACT

In this paper, a version of hybrid of Gibbs point process models is proposed as method to characterise the multiscale interaction structure of several seismic sequences occurred in the Eastern Sicily in the last decade. Seismic sequences were identified by a clustering technique based on space-time distance criterion and hierarchical clustering. We focus our analysis on five small seismic sequences, showing that two of these are described by an inhomogeneous Poisson process (not significant interaction among events) while the other three clusters are described by a Hybrid-Geyer process (mutiscale interaction between events). The proposed method, although it still needs extensive testing on a larger catalogue, seems to be a promising tool for the characterization of seismogenic sources through the analysis of induced seismicity.

1. INTRODUCTION

Given an area observed during a time interval, earthquakes can be considered as a realization of a marked space-time point process, assuming that each event, with a given magnitude (the mark), is identified by a point in space (by its geographical coordinates) and time (fixing its time of occurrence).

Generally in the point process theory, the attention is focused on two complementary aspects that can be untangled with summary statistics and model formulations [Diggle, 2013; Baddeley et al., 2015]. The first aspect is the description of the first-order characteristics of the point process estimating the intensity function; whilst the second aspect concerns the description of the events dependence, and so of the second-order properties of the process. In a given pattern, the events may exhibit regularity (where points tend to avoid each other), independence (complete spatial randomness), and clustering (where points tend to be close together).

To describe real point process phenomena, like seismic events, more complex models than the stationary Poisson that assumes statistical independence of events are defined. Indeed, seismic data represent an interesting situation where the study and the interpretation of features like self-similarity, long-range dependence and fractal dimension are crucial.

Moreover, the distribution of epicentres generally shows diverse interaction structures at different spatial and spatio-temporal scales varying according to the location of earthquake sources in the study area.

Therefore, the study of the second-order properties of a point process has a relevant role in the comprehension of the process and its realization.

Earthquakes are typically observed as clusters in space and time. In space, earthquakes epicentres are typically highly concentrated along the plate boundaries and, in general, along active faults [Baddeley et al.,

2015]. On the other hand, clustering in time can be seen as a significant increase of seismic activity immediately after large earthquakes leading to aftershock sequences.

Currently in the seismological context when events are clustered together, the modelling formulation is usually based on self-exiting point processes assuming that the occurrence of an event increases the probability of occurrence of other events in time and space (such as the Hawkes model, Hawkes and Adamopoulos [1973] or the Epidemic Type Aftershock-Sequences (ETAS) model, Ogata [1988]).

Although the models cited above represent a wide variety of solutions to describe different types of spatio and spatio-temporal patterns, more complex models need to account for environmental heterogeneity while detecting interactions at several spatial scales (multiscale dependences). For this reason, it is attractive and motivating the definition and estimation of models that account for both attractive and repulsive dependences, such as the Hybrid of Gibbs models [Baddeley et al., 2013], while also including the effect of observed covariates in order to better describe the probability of occurrence of earthquakes in fixed regions. Siino et al. [2017] provide a novel contribution to the literature on point processes and seismological applications using a hybrid approach and the distance to seismic sources as covariates for the analysis of earthquakes in the Hellenic area.

In this paper, we try to characterize the interdependence of events occurred, at several spatial scales, in the East Sicily area. Indeed, an accurate study of the moderate and small seismicity of the Eastern Sicily could be useful to better understand the seismogenic sources of this area. For this reason, starting from a seismic catalogue over the last decade, we identify some sequences and we analyze their spatial distribution with a point process approach.

In particular, we describe the spatial seismicity of the selected clusters using an advanced spatial point process model formulation based on the hybrid of Gibbs processes [Baddeley et al., 2013; Siino et al., 2017]. The main characteristics of Hybrid of Gibbs models is that it is possible to describe the multiscale interaction between the points in presence of larger scale inhomogeneity. Therefore, in this paper, after describing each sequence in terms of the previous model, the results are related to the underlying geological information of the studied areas and some comparisons are done.

The paper is organized as follows. Section 2 presents a review of the main geological and seismic characteristics of the Eastern Sicily. The methodological methods used to select clusters are explained in Section 3. The model formulation used in this paper is reported in Section 4. The results of the analysis and the estimated models are presented in Section 5.

The last section is devoted to conclusions and final remarks.

2. SETTING: THE STUDY AREA

East Sicily and South Calabria is the area with greater deformation rate and seismic strain release in Italy [Serpelloni et al., 2010; Palano, 2015]. In this area, the Nubia and Eurasia plates collide, giving birth to a complex tectonic puzzle dominated by a NNW-SSE-oriented convergence where also crustal extension and strike-slip zones coexist in a relative small region [Hollenstein et al., 2003; Serpelloni et al., 2007; Caporali et al., 2009], see Figure 1.

Two main zones of crustal contraction are located in the Tyrrhenian Sea, and at the front of the Calabrian Arc in the Ionian Sea [Billi et al., 2007; Lavecchia et al., 2007; Giunta et al., 2009; Polonia et al., 2011, 2012] characterized by compressional directions roughly transversal to the chain axis. They all are limited by a strike-slip transfer zone extending from the Aeolian Islands to the Malta escarpment [Palano et al., 2012; Polonia et al., 2012; Gallais et al., 2013; Orecchio et al., 2014]. Eastern Sicily and southern Calabria are affected by crustal extension mainly WNWESE oriented whose origin has been related to different tectonic processes [Tortorici et al., 1995; Monaco et al., 1997; Catalano et al., 2008; De Guidi et al., 2012]. All these domains are well documented at local scales by the occurrence of active fault segments, marine terracing, growing folds and active basins [Catalano and De Guidi, 2003; Bianca et al., 1999, 2011; Catalano et al., 2011; Sulli et al., 2013; Argnani et al., 2013; De Guidi et al., 2013].

The area is therefore characterized by a high variability of tectonic regimes and trajectories of the tectonic stress field [Montone et al., 2012; Pierdominici and Heidbach, 2012; De Guidi et al., 2013; Presti et al., 2013; Scarf et al., 2013; Palano et al., 2015]. Such complexity is also testified by recent tomographies: large Vp anomalies in the crust structure are well depicted and reflect the articulated crustal structure [Neri et al., 2012; Presti et al., 2013; Musumeci et al., 2014; Palano et al., 2015; Scarf et al., 2016; D ╒Alessandro et al., 2016].

Moderate and small crustal earthquakes are di used throughout the whole area, well marking the active zones aforementioned and with coherent seismogenic stress orientation [Neri et al., 2005; Scarf et al., 2013; Presti et al., 2013]. Deep seismicity marks the eastern Aeolian Island sector and the Tyrrhenian o shore of the Calabria; here deep seismicity (down to 450 km) is reported and is in-

terpreted as the subducing Ionian slab under the Calabrian Arc [Selvaggi and Chiarabba, 1995; Chiarabba et al., 2005].

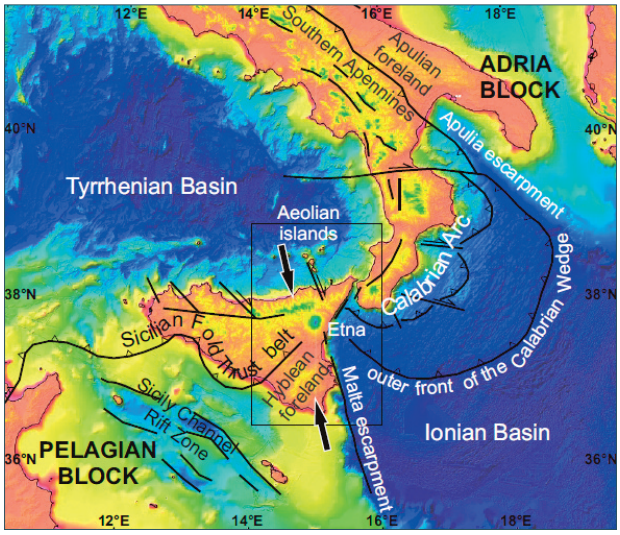

FIGURE 1. Geodynamic setting of the central Mediterranean area; main lineaments are drawn after Catalano et al. [2008]; Del Ben et al. [2008]; Polonia et al. [2011]; the big arrows represent the direction of the active convergence in Sicily, and the box indicates the study area.

In historical time, the whole area experienced several $M > 7.0$ earthquakes that caused surface faulting, tsunamis, and large landslides [Guidoboni et al., 2007; Locati et al., 2011; Tinti et al., 2004]. Some authors framed all the large earthquakes in a single regional fault system [Neri et al., 2006; Catalano et al., 2008] running roughly N-S for about 370 km and consisting in a belt of several normal fault segments controlled by a WNW-ESE local extension confirmed either from structural analysis [Monaco et al., 1997; Catalano et al., 2008; De Guidi et al., 2013] and geodetic measurements [D'Agostino and Selvaggi, 2004]; however the situation is likely to be more complex. If in the southern Calabria the seismic sources of such large earthquakes were somehow recognized [Tortorici et al., 1995; Neri et al., 2006; Galli and Bosi, 2002; Jacques et al., 2001; Catalano et al., 2008; Galli and Peronace, 2015], the seismic sources of the most destructive earthquakes in the eastern Sicily are still controversial. In particular, several different possible faults, with different geometry and kinematics, were proposed for the two largest earthquakes that stroke Sicily in the last centuries: 1693 South Eastern Sicily (M = 7.5) and 1908 (M = 7.1) Messina Straits earthquakes.

As seismogenic source of the former was proposed a normal fault in the near offshore of eastern Sicily (Bianca et al., 1999), a thrust fault at the front of the Sicilian belt [Azzaro and Barbano, 2000; Barbano and Rigano, 2001], and a subduction fault plane in the Ionian basin [Gutscher et al., 2006].

The seismogenic source of the Messina earthquake is debated although the epicentral area, and the focal mechanism are somehow well constrained [Pino et al., 2000, 2009]. The different fault plane solutions proposed in the literature are somehow coherent each other, suggesting a roughly NNE-SSW to SSE-NNW trending structure with prevailing extensional motion. However, the dip directions are sometime opposite and angles variable; in fact some authors propose various west-dipping faults in the Calabrian side of Messina Straits [Schick, 1977; Bottari et al., 1986; Catalano et al., 2008; Aloisi et al., 2013], while some others propose east-dipping structures in the Sicilian side [Capuano et al., 1988; Boschi et al., 1989; De Natale and Pingue, 1991; Valensise and Pantosti, 1992; Amoruso et al., 2002; Neri et al., 2004; Valensise et al., 2008; Bonini et al., 2011].

Similarly, many other strong earthquakes in eastern Sicily during historic time were not associated reliably and unequivocally to a seismogenic fault: 1542 (M = 6.6), 1624 (M = 5.6), 1818 (M = 6.2), 1848 (M = 5.5), and 1990 (M = 5.3) [Basili et al., 2008; Rovida et al., 2016]. The knowledge of the seismic sources is inevitably poorer in the Ionian and Tyrrhenian offshore where only in the very last years some more accurate studies were carried out [Argnani et al., 2009; Polonia et al., 2011, 2012; Cultrera et al., 2017; Gutscher et al., 2016].

2.1 INSTRUMENTAL SEISMICITY

In the following statistical analyses, each seismic event will be considered as a point in the space individuated by its three spatial coordinates (latitude, longitude, depth). Of course an earthquake source should be considered as a volume rather than a single point source; furthermore, earthquake location is affected by errors, but we can assume that all the errors associated to all the single events average out each other when they are treated together. The errors represent the standard confidence interval, expressed in km, of the horizontal and vertical coordinates after the localization of the event has been calculated. They depend partly on the capability of the seismic network and partly on the reliability of the velocity models.

However, to avoid the coarser earthquake location, we considered the seismic catalogue only since 2006, when the Italian National Seismic Network was upgraded and earthquake location was sensibly improved, the average errors are 0.85 km and 0.76 km for the horizontal and vertical coordinates, respectively.

The study area is focused on eastern Sicily: it extends

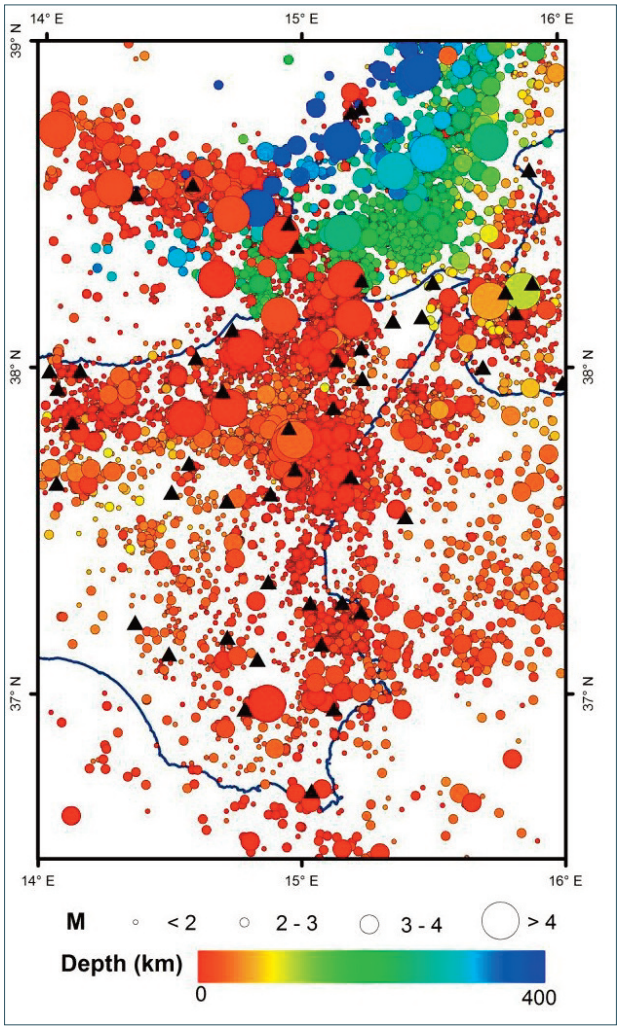

FIGURE 2. The seismicity map of the study area during the 2006 - 2016 period, black triangles indicate the seismic stations.

from 36:5 to 39 Lat. N and from 14 to 16 Long. E. The instrumental seismicity of the area, recorded in the period from 2006 to 2016, consists of 12356 events (http://cnt.rm.ingv.it/); 7825 events (63.3%) have $M < 2$, 4170 events (33.7 %) have M between 2.1 and 3.0, 333 events (2.7 %) have M between 3.1 and 4.0, and just 28 events (0.2 %) have $M > 4$ (Figure 2). The most of the events (9313, 75.4%) are crustal, with hypocentral depth lower than 30 km. In detail 4824 events (39%) are shallower than 10 km, 5530 events (44.7%) have hypocentral depth comprises between 10.1 and 50 km, 1789 events (14.4%) have hypocentral depth comprises between 50.1 and 200 km, 213 events (1.7%) are deeper than 200 km (Figure 2). The magnitude of completeness of the catalogue is $M_c = 2.3$, considering the empirical frequency-magnitude distribution (FMD) [Mignan and Woessner, 2012]. The corresponding estimate of the b parameter of the Gutenberg-Richter law obtained with moment estimator on transformed data is 1.06.

3. CLUSTER DETECTION

Instrumental seismicity can be generally distinguished into independent earthquakes (back-ground seismicity) and dependent earthquakes, like aftershocks, foreshocks, (events that occurs before and after a larger seismic event called mainshock, and related to it both in time and space) or multiplets. The process of splitting events of a seismic catalogue in background seismicity and dependent earthquakes is generally called seismic declustering [Van Stiphout et al., 2012]. Seismicity declustering is fundamental process in order to better study the seismicity characteristic and seismogenetic structure interaction, for seismic hazard assessment and in earthquake prediction models. While the identification of multiplets, characterized by very similar waveforms [Adelfio et al., 2012; D'Alessandro et al., 2013] is a simple task, the identification of foreshock and aftershock is more complicated because they cannot be distinguished by any particular outstanding feature in their waveforms. The identification of seismic sequences, foreshock-mainshock-aftershock is only possible after the full sequence of events has happened on the basis of their spatio-temporal proximity to each other. In the last decades, a lot a declustering techniques was proposed [Van Stiphout et al., 2012] almost all based to the definition of a measure of the space-time distance between earthquakes. One of the most simple procedure for identifying aftershocks within seismicity catalogues was introduced by Gardner and Knopo [1974]. In this method, widely known as the "Window Method" (WM), the identification of dependent earthquakes is based on the determination and analysis of an inter-event distance in time and space. Since this first work, a lot of declustering methods based on similar principle were proposed [Reasenberg, 1985; Uhrhammer, 1986; Frohlich and Davis, 1990; Molchan and Dmitrieva, 1992]. In WM, foreshocks and aftershocks are treated in the same way. For each earthquake in the catalogue with magnitude M, previous or subsequent shocks are identified as foreshock or aftershocks, respectively, if they occur within a specified time interval $T(M)$, and within a distance interval $L(M)$, whose width is clearly function of the mainshock magnitude. Frohlich and Davis [1990] proposed a simple criteria to define a space-time distance between two earthquakes i and j

$$d_{ij} = \sqrt{r_{ij}^2 + C^2 t_{ij}^2} \qquad (1)$$

where r_{ij} is the distance between the hypocentres, t_{ij} is the absolute difference between the event origin time and C is a scaling constant. Two earthquakes i and j are

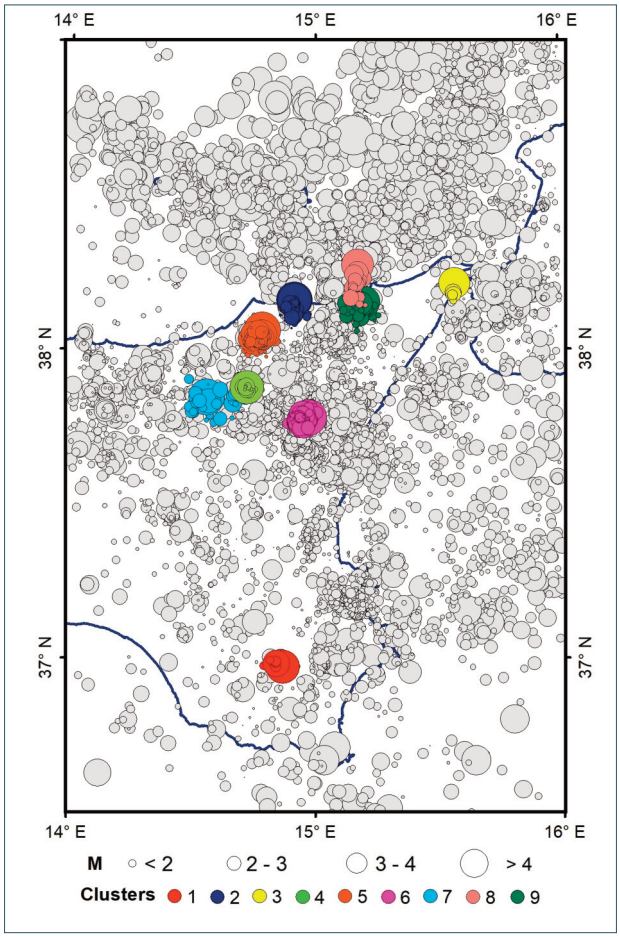

FIGURE 3. The distribution of the detected clusters. The selected clusters refer to the sequences of events occurred in the neighbourhood of these places: Palazzolo Acreide in 2016, (2) Patti in 2013, (3) Messina in 2013, (4) San Teodoro in 2013, San Salvatore di Fitalia in 2011, (6) Maletto in 2009, (7) Cerami in 2009, (8) Milazzo in 2007 and (9) Barcellona Pozzo di Gotto in 2006.

considered depended if $d_{ij} < D$, where D is a time-space distance threshold to optimize on the basis of the analysis of the background activity of the study region.

According to Davis and Frohlich [1991] in Equation (1), we set $C = 1\ km/day^{-1}$ while in this paper we suggest a different procedure for threshold optimization based on Agglomerative Hierarchical Cluster (AHC) algorithm [Gan et al., 2011; Everitt et al., 2011; D'Alessandro et al., 2013, 2016; Martorana et al., 2016].

In the clustering procedure, we adopt the Average Linkage (AL) criterion while the dendrogram cut level was determined using internal entropy level criterion to maximize the homogeneity within classes Celeux and Soromenho [1996]. After the clustering procedure, we identified nine clusters (Figure 3), and their characteristics are summarized in Table 1.

4. SPATIAL POINT PROCESS MODELS

In this section, we explain the basic concepts of a spatial point process describing its first- and second-order properties. Moreover, the Gibbs processes and their hybrid formulation are introduced explaining how to fit these models to data, to assess the goodness of fit and how to interpret the main parameters. Definitions and notations used throughout this section are introduced in Illian et al. [2008] and Baddeley et al. [2015].

A spatial point pattern $\upsilon = \{\mathbf{u}_1,...\mathbf{u}_n\}$ is an unordered set of points in the region $W \subset \mathbf{R}^d$ where $n(\upsilon) = n$ is the number of points, $|W| < \infty$ and usually $d = 2$. A point process model assumes that υ is a realization of a finite

		Mainshock						
Cluster id	n	M*	tM*	Lat/Long	Depth(km)	t_0	t_1	days
1	32	4.2	2016.02.28	36.97/14.87	7	2016.02.06	2016.03.13	36
2	435	4.4	2013.08.15	38.16/14.91	26	2013.01.12	2013.12.19	341
3	42	4	2013.12.23	38.22/15.57	10	2013.12.23	2014.04.04	103
4	70	4.2	2013.01.04	37.88/14.72	15	2012.10.19	2013.01.21	94
5	414	4.5	2011.06.23	38.06/14.78	7	2011.06.11	2011.11.14	156
6	150	4.4	2009.12.19	37.78/14.97	27	2009.12.18	2010.09.21	277
7	56	4.4	2009.11.08	37.85/14.56	8	2009.06.08	2010.10.23	502
8	55	4.1	2007.08.18	38.28/15.17	11	2007.04.25	2007.10.06	164
9	88	4.1	2006.02.27	38.26/15.2	9	2005.12.19	2007.04.16	483

TABLE 1. Summary information relative to the nine selected clusters: number of events n, details of the mainshock (magnitude M^*, date t_{M^*}, latitude, longitude and depth), start and end dates of the sequence (t_0 and t_1) and days extension of each cluster.

point process X in W without multiple points. The first-order property of X is described by the intensity function. It is defined as

$$\rho(\mathbf{u}) = \lim_{|d\mathbf{u}|\to 0} \frac{E(Y(d\mathbf{u}))}{|d\mathbf{u}|} \quad (2)$$

where $d\mathbf{u}$ is an infinitesimal region that contains the point $\mathbf{u} \in W$, $|d\mathbf{u}|$ is its area and $E(Y(d\mathbf{u}))$ denotes the expected number of events in $d\mathbf{u}$. When the intensity in Equation (2) is constant the process is called homogeneous. On the other hand, in the inhomogeneous case the intensity is not constant in the study area, but may depend, for instance, on the coordinates of points, still assuming independence of the past. A Poisson process model, which assumes that the random points are independent of each other, is completely described by its intensity function $\rho(\mathbf{u})$.

The interpoint interaction between events is measured by second-order moment quantities. Several functional summary statistics are used to study the second-order characteristics of a point pattern and so measuring dependence. Two widely used summary statistics, for descriptive analysis and diagnostics, are the Ripley's K-function and G-function (also called nearest-neighbour distance distribution function) [Ripley, 1976, 1988].

Knowing that, in a stationary process the distribution of X is the same as the distribution of the shifted process $X + v$, for any vector v, the K-function is defined as

$$K(r) = \frac{1}{\rho} \boldsymbol{E} \text{ [number of } r\text{-neighbours of } \mathbf{u} | X \text{ has point at location u]} \quad (3)$$

for any distance $r \geq 0$ and any location u. When the process is stationary, the most commonly used estimator for (3) is due to Ripley [1976] is

$$\hat{K}(r) = \frac{|W|}{n(n-1)} \sum_{i=1}^{n} \sum_{j=1, i\neq j}^{n} I(d_{ij} \leq r) w(\mathbf{u}_i, \mathbf{u}_j) \quad (4)$$

where n is the number of points in the pattern, $|W|$ is the area of the window, $w(\mathbf{u}_i, \mathbf{u}_j)$ is the Ripley's edge correction weight and $d_{ij} = ||\mathbf{u}_i - \mathbf{u}_j||$ is the pairwise distances between all distinct pairs of points $\mathbf{u}_i$ and $\mathbf{u}_j$ in the pattern.

The G-function is the cumulative distribution function of the nearest-neighbour distance at a typical point of X. It is a function of $d_i = d(\mathbf{u}_i, \upsilon \backslash \mathbf{u}_i)$ that indicates the shortest distance from $\mathbf{u}_i$ to the pattern $\upsilon \backslash \mathbf{u}_i$ consisting of all points of υ except $\mathbf{u}_i$. It is defined as

$$G(r) = \boldsymbol{P}\{d(\mathbf{u}, X \setminus \mathbf{u} \leq r) / X \text{ has a point in } \mathbf{u}\} \quad (5)$$

for any distance $r \geq 0$ and any location $\mathbf{u}$. The estimator of (5) is based on the empirical cumulative distribution functions of the nearest-neighbour distances at all data points. $G(r)$ is a non-decreasing step function and $G(0) = 0$. Under the homogeneous Poisson assumption the following theoretical relations hold

$$K(r) = \pi r2 \text{ and } G(r) = 1 - \exp(-\rho\pi r^2).$$

Visual inspection of empirical K-function (G-function) with the theoretical summary statistic of the homogeneous Poisson process is used to study correlation in a descriptive analysis of the data.

4.1 GIBBS AND HYBRID OF GIBBS POINT PROCESS MODELS

Gibbs point process is a class of flexible and natural models for point patterns that postulates interactions between the points of the process defining a density for a point process with respect to a Poisson process of unit intensity [Møller and Waagepetersen, 2003].

The class of Gibbs processes X, also called Markov point processes, is determined through a probability density function $f : < X \to [0, \infty)$,
where $X = \{\upsilon \subset W : n(\upsilon) < \infty\}$ is a set of point configurations contained in W. In the literature several Gibbs models have been proposed such as the area-interaction, Strauss, Geyer, hard core processes [Møller and Waagepetersen, 2003]. For further details on them and on the desirable properties for an unnormalized density see Møller and Waagepetersen [2003] Baddeley et al. [2013] and Baddeley et al. [2015]. We explain with more detail the Geyer process and the interpretation of its parameters in terms of interaction between the points, since Geyer models are used mainly when the aim is to study attractive interaction among points. The unnormalized density of the Geyer saturation process [Geyer, 1999] is equal to

$$f(v) = \beta^{n(v)} \prod_{i=1}^{n(v)} \gamma^{\min(s, t(\mathbf{u}_i, v \backslash \mathbf{u}_i))} \quad (6)$$

where $s > 0$ is the saturation parameter and $t(\cdot)$ is the number of unordered pairs of distinct points in the pattern υ that lie closer than r units apart. When in Equation (6) the s is set to infinity, this model reduces to the Strauss process with interaction parameter γ^2. Instead if $s = 0$, the model reduces to the Poisson point process. If s is a finite positive number, then the interaction parameter γ may take any positive value. The process is inhibitive when $\gamma \leq 1$, and clustered when $\gamma > 1$.

However, Gibbs processes have some drawbacks when points have a strong clustering and show spatial dependence at multiple scales [Illian et al., 2008; Møller and Waagepetersen, 2003; Baddeley et al., 2013].

Baddeley et al. [2013] proposes hybrid models as a

general way to generate multi-scale processes combining Gibbs processes. Given m unnormalized densities $f_1, f_2, ..., f_m$ the hybrid density is defined as $f(\upsilon) = f_1(\upsilon)$ x...x $f_m(\upsilon)$, respecting some properties. For example the density of the stationary hybrid process obtained considering m Geyer components (3) (with interaction ranges $r_1, ...r_m$ and saturation parameters $s_1, ..., s_m$) is

$$f(v) = \beta^{n(v)} \prod_{i=1}^{n(v)} \prod_{j=1}^{m} \gamma_j^{\min(s_j, t(\mathbf{u}_i, v \setminus \mathbf{u}_i; r_j))} \quad (7)$$

where $t(\mathbf{u}_i, \upsilon\setminus\mathbf{u}_i; r_j) = \sum_i \{\mathbf{1}\| \mathbf{u} - \mathbf{u}_i \| \le r_j\}$. This density indicates that the spatial interaction between points changes with the distances r_j and the parameters that capture this information are the interaction parameters γ_j. If an inhomogeneous version of (7) is considered, the parameter β is replaced by a function $\beta(\mathbf{u}_i)$ that expresses a spatial trend and it can be a function of the coordinates of the points and covariate information defined in all the study area. Generally, we can specify that the density f is a function of a vector of regular parameters θ and a vector of irregular parameters η. In the case of (7), the previous two parametric vectors are
$\theta = \{\log(\beta), \log(\gamma_m)\} = \{\theta_1, \theta_2\}$ for regular parameters and $\eta = \{(r_1, s_2), ..., (r_m, s_m)\}$ for the irregular ones. Moreover, the regular vector can be subdivided into parameters for the description of the spatial trend (θ_1) and parameters for the interaction effects (θ_2).

Gibbs models can be fitted to data by pseudolikelihood (composite likelihood) [Besag, 1975, 1977; Jensen et al., 1991], and it is function of the Papangelou conditional intensity $\rho_\phi(\mathbf{u}|\upsilon)$ at location $\mathbf{u} \in W$ given υ, where ϕ are the parameters to estimate. In hybrid models $\phi = \{\theta, \eta\}$ and the conditional intensity is the product of the conditional intensities of the components [Baddeley et al., 2013]

$$\rho_\phi(\mathbf{u}, v) = \exp\{\mathrm{B}(\mathbf{u}) + \theta_1^T \mathrm{V}_1(\mathbf{u}, \eta) + \theta_2^T G(\mathbf{u}, v, \eta)\} \quad (8)$$

where $B(\mathbf{u})$ is an offset term, $\theta_1^T V_1(\mathbf{u}, \eta)$ is the first-order potential and $\theta_2^T V_1(u, \upsilon, \eta)$ is the sum of terms with $k \ge 2$. The term $G(\cdot)$ accounts for the interaction effects, and in the following analysis, it will be a combination of Geyer processes. The irregular parameters are estimated through the profile pseudolikelihood, maximizing $p(\eta, \upsilon) = \max_\theta \log PL(\theta, \eta)$ over η. For details for computing approximate maximum pseudolikelihood estimates see Baddeley and Turner [2000]. Different specifications can be considered for the trend part $B(\mathbf{u})$ and $\theta_1^T V_1(\mathbf{u})$ of (8). We consider a non-parametric formulation for the spatial term depending on the coordinates using kernel estimators [Silverman, 1986].

4.2 DIAGNOSTICS FOR THE HYBRID MODELS

Diagnostics is based on a graphical approach, involving also the residual K- and G-functions [Baddeley et al., 2011]. Moreover, we compare and assess the goodness-of fit of the estimated models in terms of AIC, spatial raw residuals and number of simulated points under the estimated model [Baddeley et al., 2005]. Furthermore, the diagnostic plots based on the residual K- and G-functions are used to decide which component has to be added at each step to the hybrid model.

The residual K-function (G-function) with respect to a fitted model is a modification of the K-function which has mean equal to zero if the model is true. Indeed, these graphs show for which spatial distances the current model has a lack of fit in describing the interaction between points. The residual K-function for a fitted model, evaluated at a specific distance r, is the score residual used for testing the current model against the alternative of the current model plus a Strauss process with the same trend and with interaction distance r.

Similarly, the residual G-function for a fitted model, evaluated at a given r, is the score residual used for testing the current model against the alternative of a Geyer saturation model with saturation parameter 1 and interaction radius rr Baddeley et al. [2011]. In the analysis, for model selection and to assess the goodness of fit, we computed both the residual G and K-functions and in section 5 we report the graphs for the residual G-functions of the estimates inhomogeneous Poisson models and hybrid of Gibbs process models. In the spatstat package [Baddeley and Turner, 2005] of R [R Development Core Team, 2005], there are most of the functions that have been used for fitting, prediction, simulation and validation of Hybrid models.

5. RESULTS

The models introduced in Section 4 are fitted to the largest sequences 2, 4, 5, 6 and 9 (at least 70 events), see Table 1.

For each sequence, the magnitude of completeness M_c is estimated with a visual evaluation, and in a conservative way, of the empirical frequency-magnitude distribution (FMD) and events of magnitude $M < M_c$ are discarded [Mignan and Woessner, 2012].

Table 2 shows for the selected clusters, the value of M_c and the corresponding estimate of the b parameter of the Gutenberg-Richter law obtained with moment estimator on transformed data.

Such parameters are useful to characterize the clusters, to compare them each other, and, partially, with

Cluster id	M_c	n	b
2	1.5	130	0.89
4	1	68	0.59
5	1	394	0.57
6	2	124	0.68
9	2	54	0.80

TABLE 2. Magnitude of completeness (M_c) and n indicates the corresponding number of events in the sequence. b is the estimated parameter of the Gutenberg-Richter law.

the background seismicity (i.e. the whole catalogue).

The b-value of the earthquake frequency-magnitude distribution generally ranges between 0.8 and 1.1; variations are associated to several aspects, e.g. fracturing degree, material properties, stress concentration degree, pore-fluid pressure, tectonic setting, and to the petrological-environmental-geophysical characteristics [El-Isa and Eaton, 2014].

While the b-values of the clusters could be indicative of these local conditions, the corresponding values for the catalogue (b = 1.06) results from the combination of a multiplicity of geological/geodynamic conditions and, in this perspective, it is not useful to discuss about. Probably there is not a significant reason for the b-values of the clusters being always lower than b-value of the whole catalogue. Small b-values (0.7 - 0.4) are generally associated to intra-plate seismicity or, for small magnitudes, to the incompleteness of the catalogues. Cluster 4, 5, and 6 show lower b-values (0.6-0.7). Excluding the incompleteness of the catalogue, low b-values for these three clusters can be related to the local geological and tectonic context that may influence the real state of stress. For descriptive purposes, the summary statistics K- and G-functions are estimated for each cluster assuming stationarity, and we report the estimation of the last summary statistics. In Figure 4, for each sequence, the nearest neighbour distance distribution function (black line) and the true value of G for a stationary completely random point process (red line) together with the envelopes considering 39 simulations under CSR assumption are compared. For the clusters 2, 4, 5 and 6, we observe remarkable deviations between the empirical and theoretical G curves, and this behaviour indicates spatial clustering. However, for the cluster 9, the curve is inside the envelope except for distances less than 0.5 km. The graphical output obtained with the estimated K-functions and the related envelopes under the CSR assumption are not reported and they are coherent with the previous results. However, we want to point out that generally a summary function does not completely characterize a point process and the G- and K-functions are sensitive to different aspects of the point process. In particular, the G-function summaries information at a shorter scale than the K-function [Baddeley et al., 2015].

Cluster id	Method	$h=\{h_x,h_y\}$
2	Scott	(0.577; 0.915)
4	FLP	(0.455; 0.348)
5	Scott	(0.688; 0.611)
6	Scott	(0.680; 0.748)
9	Diggle	(0.429; 0.429)

TABLE 3. Vector of the selected smoothing bandwidths in the x and y directions for the kernel estimation of an inhomogeneous Poisson process intensity obtained with the specified method.

For each cluster, the first attempt in model estimation is to fit an inhomogeneous Poisson model with intensity depending on the spatial coordinates in which points do not interact with each other. We consider a non-parametric formulation for the spatial term in (5), considering kernel estimators with respect to the Cartesian coordinates and a null value for the interaction term.

To determine the smoothing bandwidth for the kernel estimation of point process intensity several methods have been proposed in the literature: Scott's rule, cross-validation, FLP (Forward Likelihood for Prediction) approach [Chiodi and Adelfio, [2017]; Adelfio and Chiodi, [2015]]. For each cluster, the best bandwidth has been selected considering the inhomogeneous Poisson model with the smallest AIC. Table 3 shows the used method to estimate the smoothing bandwidth vector and the corresponding values for each cluster ($\mathbf{h} = \{h_x, h_y\}$).

The corresponding AIC and the range of the spatial raw residuals of the fitted inhomogeneous Poisson models are in Table 4. Given the point process models fitted to the point patterns, the residual K- and G-functions are used as diagnostic tools to assess the goodness-of-fit of the models [Baddeley et al., 2011]. In Figure 5, the residual G-functions for the estimated inhomogeneous

	Inhom. Poisson mode			Inhom. Hybrid of Gibbs processes			
id	AIC	Range res.	Comp.	η	γ	AIC	Range res.
2	-141.375	[-0.347 ; 0.665]	G1	(r1;s1) = (0.200 ; 3.5)	1.295	-168.060	[-0.223 ; 0.245]
4	-70.735	[-0.124 ; 0.521]	G1	(r1;s1) = (0.080 ; 0.1)	1.713	-74.128	[-0.146 ; 0.364]
5	-961.829	[-0.142 ; 0.531]	G1	(r1;s1) = (0.060 ; 0.2)	0.413	-990.565	[-0.258 ; 0.171]
			G2	(r2;s2) = (0.240 ; 3.5)	1.157		
6	-73.665	[-0.107 ; 0.533]	G1	(r1;s1) = (0.070 ; 0.5)	0.216	-95.661	[-0.094 ; 0.210]
			G2	(r2;s2) = (0.220 ; 6.0)	1.239		
9	31.031	[-0.033 ; 0.088]					

TABLE 4. Estimation results for the inhomogeneous Poisson and the selected hybrid of Gibbs models: AIC, range of spatial raw residuals, vector of irregular parameter η (an interaction distance r_j and a saturation parameter s_j for each Geyer component, G_j , j = 1,2) and interaction parameter for each Geyer component γ_j.

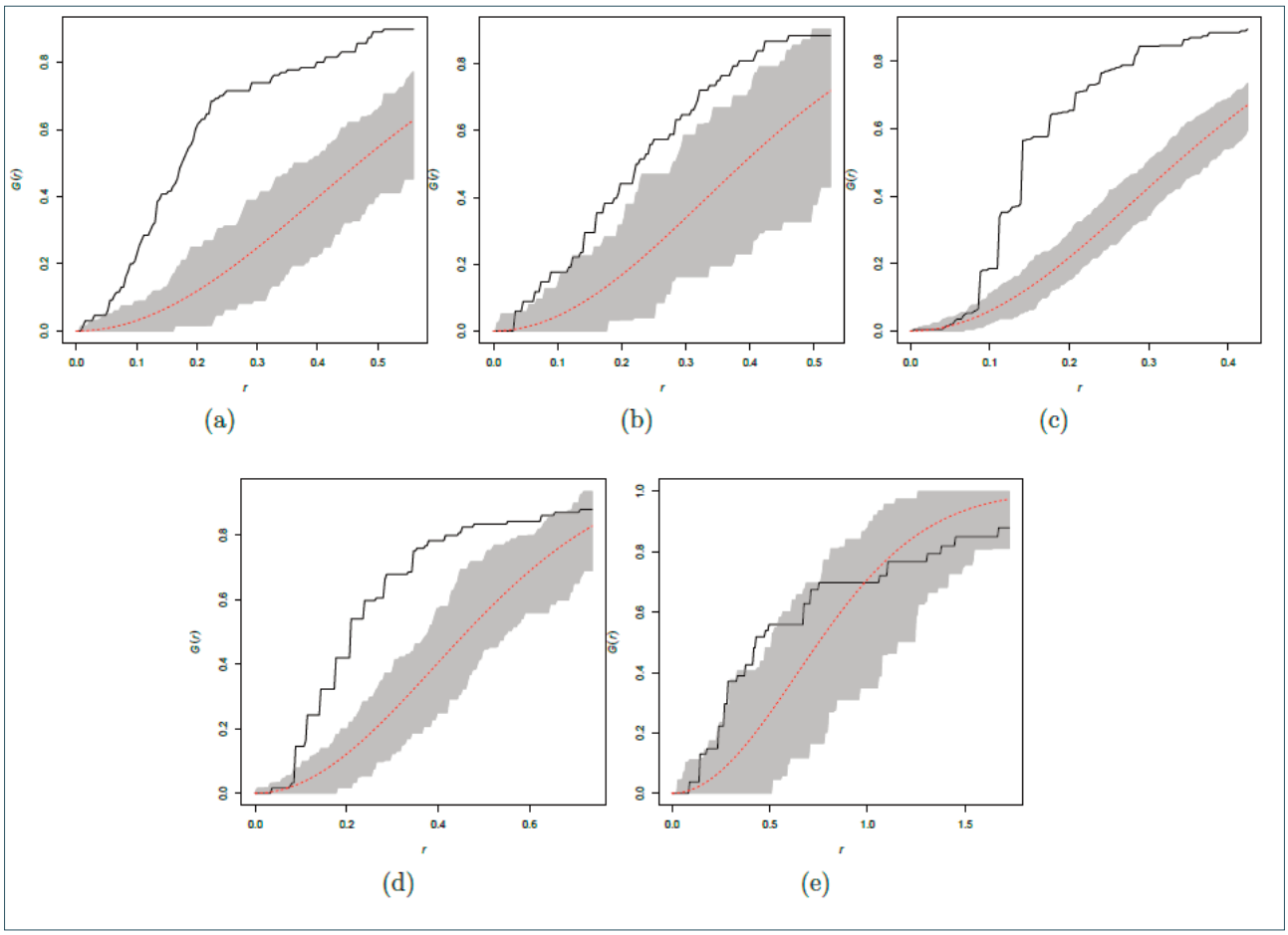

FIGURE 4. Envelope of the G-function (shaded region) to test Complete Spatial Randomness (CSR) condition. The black curve is the estimated G-function instead the red one corresponds to the function under the CSR assumption, for cluster 2 (4a), 4 (4b), 5 (4c), 6 (4d) and 9 (4e). The x-axis shows the value of distances in km.

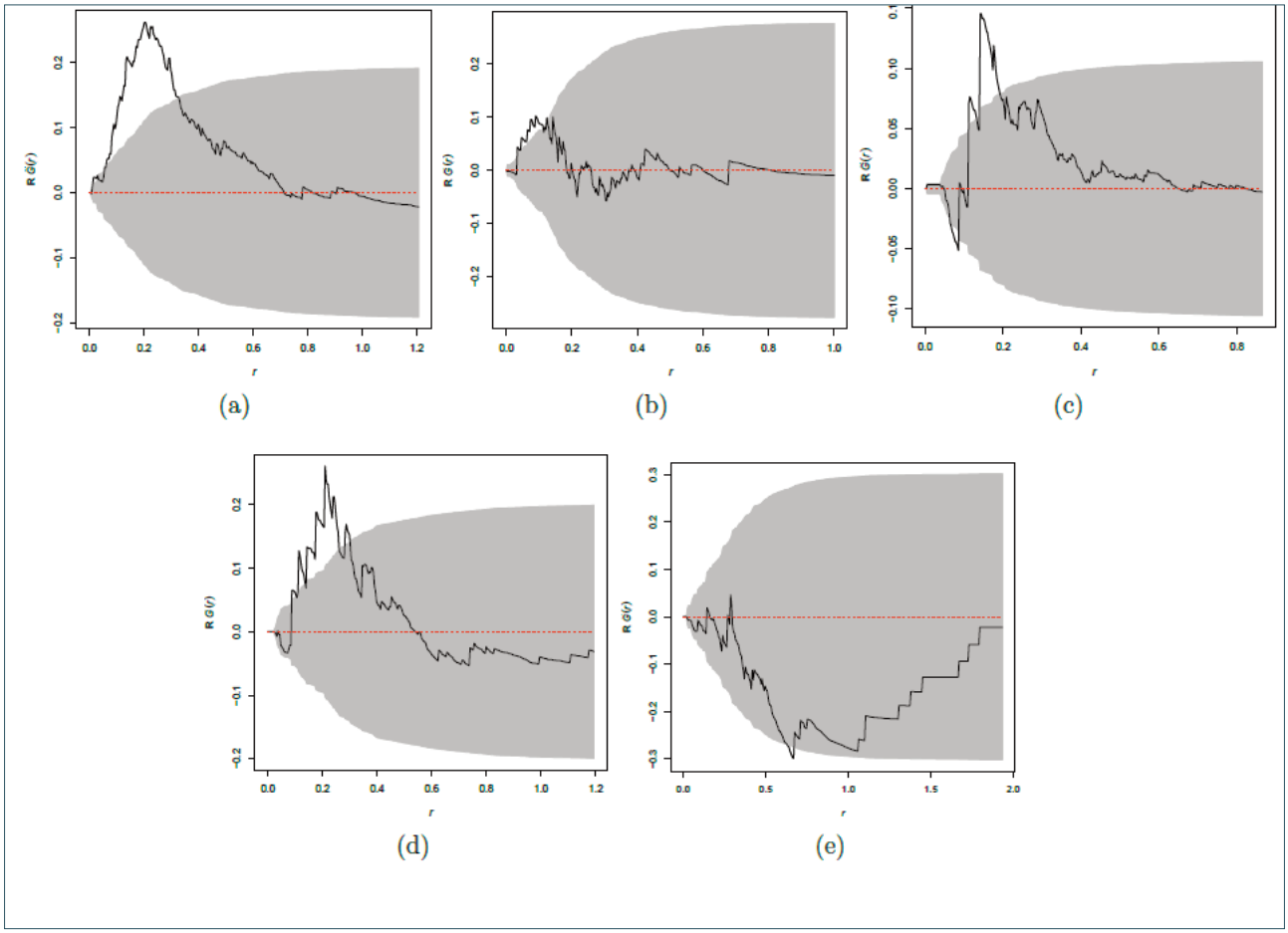

FIGURE 5. Residual G-functions for the inhomogeneous Poisson process model, fitted to cluster 2 (5a), 4 (5b), 5 (5c), 6 (5d) and 9 (5e). The x-axis shows the value of distances in km.

Poisson models are reported. For the sequences 2, 5 and 6 the residual G-functions wander substantially outside the limits showing peaks. This suggests that assuming an inhomogeneous Poisson model for those clusters is not satisfactory since there is unexplained attractive interaction between points (positive association). The sharpness of the peak for the residual G-function encourages to include a Geyer saturation process. By the way, for the sequences 5 and 6, at very short distances (less than 70 meters), the first Geyer component is similar to an inhomogeneous Poisson one, since the value of the saturation parameter s1 is close to 0 (Table 4). While, for the sequences 2, 5 and 6, for distances up to about 200 meters, a Geyer component is necessary for explaining the cluster behaviour among points: for all these clusters both the saturation parameter s and the interaction parameter are greater than 1. In particular, according to the estimated parameters, the clustering behaviour is stronger for the sequence 6.

On the other hand, we have seen before in Figure 4b and 4e that for the clusters 4 and 9, the G-functions are not so far from the CSR assumption. This is also confirmed from the residual G-functions after fitting an inhomogeneous Poisson model: in Figures 5b and 5e, the curves are not significantly far from zero. In particular, for the cluster 4, the estimated residual G-function is outside the band just for very short distances (Figure 5b), and adding a hybrid component does not seem to improve significantly the results in terms of interpretation. Indeed, the parameter $s = 0.1$ of the Geyer component (Table 4) is very low and close to zero, indicating that the added component is close to an inhomogeneous Poisson process. Instead for the cluster 9, this behaviour is more evident, since in the residual G-function (Figure 5e) there is no evidence of unexplained association in the observed data. Therefore, for this sequence an inhomogeneous Poisson process well describes the spatial inhomogeneity. Moreover, this is a very small sequence (54 earthquakes) and therefore fitting a complex model, as a hybrid one, could be misleading.

In terms of goodness of fit considering hybrid models, we have an improvement in terms of AIC and range

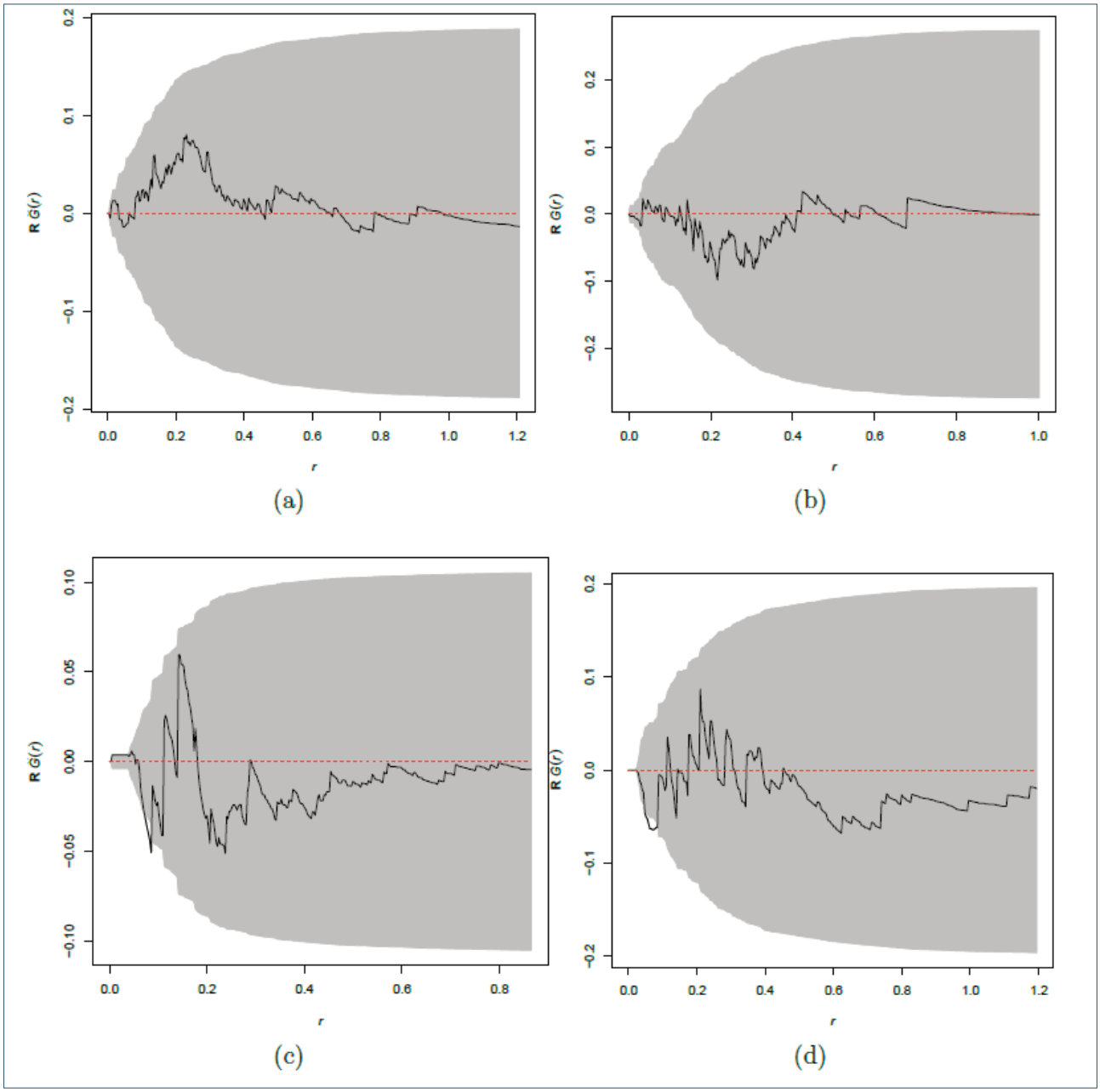

FIGURE 6. Residual G-functions for the final selected model, that is an inhomogeneous hybrid model of Geyer processes with one or two components, and parameters reported in Table 4, for cluster 2 (6a), 4 (6b), 5 (6c) and 6 (6d). The x-axis shows the value of distances in km

of spatial raw residual with respect to the inhomogeneous Poisson models (Table 4). For example, for the sequence 2 moving from an inhomogeneous Poisson model to a hybrid formulation, the AIC decreases by 26.658 and the range of the spatial raw residuals also decreases. Moreover, the residual G-functions of the final selected models (Figure 6a, 6b, 6c and 6d) oscillate around zero and they are inside the envelopes indicating that the interaction structure between the earthquakes is well described by the hybrid models.

For a visual diagnostics of the final model, we also report the images of the estimated spatial intensity for the five selected clusters, together with the observed points (Figure 7). As it can be observed, this results is also influenced by the size of clusters (see Figure 7e).

6. CONCLUSIVE REMARKS

Starting from previous results, we could say that the spatial seismicity of the sequences occurred in San Teodoro in 2013 and in Barcellona Pozzo di Gotto in

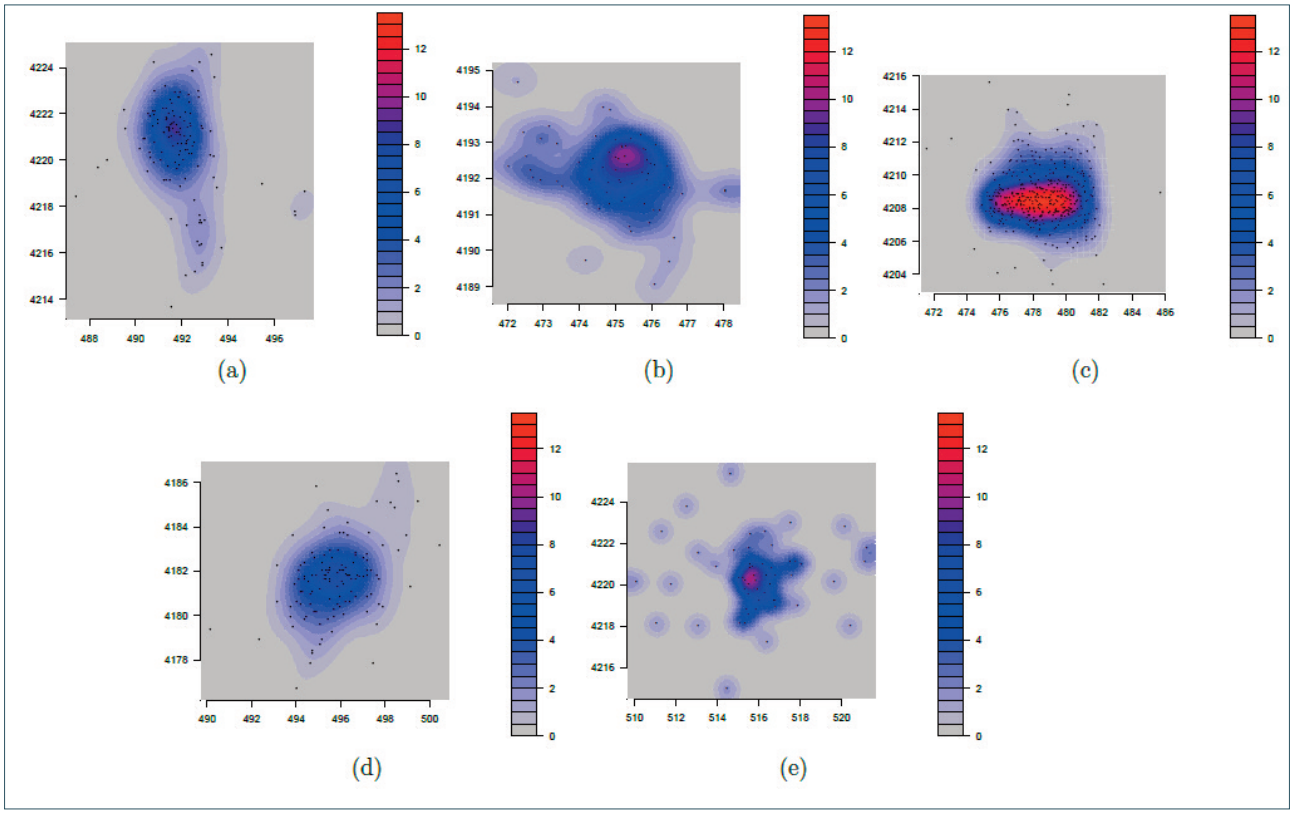

FIGURE 7. Estimated spatial intensity of the final selected model, for cluster 2 (7a), 4 (7b), 5 (7c), 6 (7d) and 9 (7e). The plots refer to Mercator projection UTM33 in km

2003 seems to be adequately described by an inhomogeneous Poisson process and, therefore, it seems that for these sets of earthquakes there is a weak interaction, i.e. a weak contagious effect between events. On the other hand, for the sequences occurred in Patti in 2013, San Salvatore di Fitalia in 2011 and Maletto in 2009, we explicitly postulate a multiscale interaction between events, fitting a hybrid of Geyer process with positive association and for distances up to 200 meters. For these last three sequences, it seems that the earthquakes occur in a more clustered behaviour. One reason for these results, and differences between the sequences, might be ascribed to the geological characteristics of the area, as the differences in the b-values among the clusters could indicate. On the other hand, to find a possible correlation of such few clusters with their positions within the complex geodynamic context of the study area, or even with the main seismogenic sources, would be a daring goal. It would be even more speculative considering that beyond the well described seismogenic structure of the study area [Basili et al., 2008] there is evidence of seismic belts not clearly associated to the well-constrained fault belt Billi et al. [2007]. Indeed, it is reasonable to assume that different seismogenic sources could be associated to seismic sequences with specific characteristics.

The errors associated to the determination of the hypocentral coordinates could have represented a limitation to the methodology, but our methodology proves to discriminate clustering effect at a multiscale level and provides promising results.

Finding possible geological explanations accounting for the differences in the clusters requires a larger catalogue and, for this purpose, application at greater scale (i.e. the whole Italy) should be performed.

Acknowledgements. This paper has been partially supported by the national grant of the Italian Ministry of Education University and Research (MIUR) for the PRIN-2015 program (Progetti di ricerca di Rilevante Interesse Nazionale), "Prot. 20157PRZC4 - Research Project Title: Complex space-time modeling and functional analysis for probabilistic forecast of seismic events. PI: Giada Adelfio".

REFERENCES

Adelfio, G. and M. Chiodi (2015). Alternated estimation in semi-parametric space-time branching-type point processes with application to seismic catalogs. Stochastic Environmental Research and Risk Assessment 29 (2), 443-450.

Adelfio, G., M. Chiodi, A. D'Alessandro, D. Luzio, G. D'Anna, and G. Mangano (2012). Simultaneous seismic wave clustering and registration. Computers & geosciences 44, 60-69.

Aloisi, M., V. Bruno, F. Cannavÿ, L. Ferranti, M. Mattia, C. Monaco, and M. Palano (2013). Are the source models of the m 7.1 1908 Messina Straits earthquake reliable? Insights from a novel inversion and a sensitivity analysis of levelling data. Geophysical Journal International 192 (3), 1025-1041.

Amoruso, A., L. Crescentini, and R. Scarpa (2002). Source parameters of the 1908 Messina Straits, Italy, earthquake from geodetic and seismic data. Journal of Geophysical Research: Solid Earth 107 (B4), ESE 4-1-ESE 4-11.

Argnani, A., G. Brancolini, C. Bonazzi, M. Rovere, F. Accaino, F. Zgur, and E. Lodolo (2009). The results of the Taormina 2006 seismic survey: possible implications for active tectonics in the Messina Straits. Tectonophysics 476 (1), 159-169.

Argnani, A., F. Mazzarini, C. Bonazzi, M. Bisson, and I. Isola (2013). The deformation offshore of Mount Etna as imaged by multichannel seismic reflection profiles. Journal of Volcanology and Geothermal Research 251, 50-64.

Azzaro, R. and M. Barbano (2000). Analysis of the seismicity of South-eastern Sicily: a proposed tectonic interpretation. Annals of Geophysics 43 (1), 171-188.

Baddeley, A., E. Rubak, and J. Møller (2011). Score, pseudo-score and residual diagnostics for spatial point process models. Statistical Science 26 (4), 613-646.

Baddeley, A., E. Rubak, and R. Turner (2015). Spatial Point Patterns: Methodology and Applications with R. London: Chapman and Hall/CRC Press.

Baddeley, A. and R. Turner (2005). Spatstat: An R package for analyzing spatial point patterns. Journal of Statistical Software 12 (6), 1-42.

Baddeley, A., R. Turner, J. Mateu, and A. Bevan (2013). Hybrids of Gibbs point process models and their implementation. Journal of Statistical Software 55 (11), 1-43.

Baddeley, A., R. Turner, J. Mђller, and M. Hazelton (2005). Residual analysis for spatial point processes. Journal of the Royal Statistical Society, Series B (Statistical Methodology) 67 (5), 617-666.

Baddeley, A. and T. R. Turner (2000). Pratical maximum pseudo likelihood for spatial point patterns (with discussion). Australian & New Zealand Journal of Statistics 42 (3), 283-322.

Barbano, M. S. and R. Rigano (2001). Earthquake sources and seismic hazard in South-eastern Sicily. Annals of Geophysics 44 (4), 723-738.

Basili, R., G. Valensise, P. Vannoli, P. Burrato, U. Fracassi, S. Mariano, M. M. Tiberti, and E. Boschi (2008). The database of individual seismogenic sources (diss), version 3: summarizing 20 years of research on Italy's earthquake geology. Tectonophysics 453 (1), 20-43.

Besag, J. (1975). Statistical analysis of non-lattice data. The Statistician 24 (3), 179-195.

Besag, J. (1977). Some methods of statistical analysis for spatial data. Bulletin of the International Statistical Institute 47 (2), 77-92.

Bianca, M., S. Catalano, G. De Guidi, A. M. Gueli, C. Monaco, G. Ristuccia, G. Stella, G. Tortorici, L. Tortorici, and S. Troja (2011). Luminescence chronology of pleistocene marine terraces of Capo Vaticano peninsula (Calabria, southern Italy). Quaternary International 232 (1), 114-121.

Bianca, M., C. Monaco, L. Tortorici, and L. Cernobori (1999). Quaternary normal faulting in southeastern Sicily (Italy): a seismic source for the 1693 large earthquake. Geophysical Journal International 139 (2), 370-394.

Billi, A., D. Presti, C. Faccenna, G. Neri, and B. Orecchio (2007). Seismotectonics of the Nubia plate compressive margin in the south Tyrrhenian region, Italy: Clues for subduction inception. Journal of Geophysical Research: Solid Earth 112 (B8).

Bonini, L., D. Di Bucci, G. Toscani, S. Seno, and G. Valensise (2011). Reconciling deep seismogenic and shallow active faults through analogue modelling: the case of the Messina Straits (southern Italy). Journal of the Geological Society 168 (1), 191-199.

Boschi, E., D. Pantosti, and G. Valensise (1989). Modello di sorgente per il terremoto di Messina del 1908 ed evoluzione recente dell'area dello Stretto. Atti VIII Convegno GNGTS, Roma , 245-258.

Bottari, A., E. Carapezza, M. Carapezza, P. Carveni, F. Cefali, E. L. Giudice, and C. Pandolfo (1986). The 1908 Messina Strait earthquake in the regional geostructural framework. Journal of geodynamics 5 (3-4), 275-302.

Caporali, A., C. Aichhorn, M. Barlik, M. Becker, I. Fejes, L. Gerhatova, D. Ghitau, G. Grenerczy, J. Hefty, S. Krauss, et al. (2009). Surface kinematics in the Alpine-Carpathian-Dinaric and Balkan region inferred from a new multi-network GPS combination solution. Tectonophysics 474 (1), 295-321.

Capuano, P., G. De Natale, P. Gasparini, F. Pingue, and R. Scarpa (1988). A model for the 1908 Messina Straits (Italy) earthquake by inversion of levelling data. Bulletin of the Seismological Society of America 78

(6), 1930-1947.

Catalano, S. and G. De Guidi (2003). Late quaternary uplift of North-eastern Sicily: relation with the active normal faulting deformation. Journal of Geodynamics 36 (4), 445-467.

Catalano, S., G. De Guidi, C. Monaco, G. Tortorici, and L. Tortorici (2008). Active faulting and seismicity along the Siculo-Calabrian rift zone (southern Italy). Tectonophysics 453 (1), 177-192.

Catalano, S., S. Torrisi, G. Tortorici, and G. Romagnoli (2011). Active folding along a rift-flank: the Catania region case history (se Sicily). Journal of Geodynamics 51 (1), 53-63.

Celeux, G. and G. Soromenho (1996). An entropy criterion for assessing the number of clusters in a mixture model. Journal of classification 13 (2), 195-212.

Chiarabba, C., L. Jovane, and R. DiStefano (2005). A new view of Italian seismicity using 20 years of instrumental recordings. Tectonophysics 395 (3), 251-268.

Chiodi, M. and G. Adelfio (2017). Mixed non-parametric and parametric estimation techniques in R package etasFLP for earthquakes' description. Journal of statistical Software 76 (1), 1-29.

Cultrera, F., G. Barreca, P. Burrato, L. Ferranti, C. Monaco, S. Passaro, F. Pepe, and L. Scarfô (2017, Apr). Active faulting and continental slope instability in the gulf of Patti (Tyrrhenian side of NE Sicily, Italy): a field, marine and seismological joint analysis. Natural Hazards 86 (2), 253-272.

D'Agostino, N. and G. Selvaggi (2004). Crustal motion along the Eurasia-Nubia plate boundary in the Calabrian Arc and Sicily and active extension in the Messina Straits from GPS measurements. Journal of Geophysical Research: Solid Earth 109 (B11), B11402.

D'Alessandro, A., D. Luzio, R. Martorana, and P. Capizzi (2016). Selection of time windows in the horizontal-to-vertical noise spectral ratio by means of cluster analysis. Bulletin of the Seismological Society of America 106 (2), 560-574.

D'Alessandro, A., G. Mangano, G. D'Anna, and D. Luzio (2013). Waveforms clustering and single-station location of microearthquake multiplets recorded in the northern Sicilian offshore region. Geophysical Journal International 194 (3), 1789-1809.

D'Alessandro, A., G. Mangano, G. D ╒Anna, and S. Scudero (2016). Evidence for serpentinizationof the Ionian upper mantle from simultaneous inversion of p-and s-wave arrival times. Journal of Geodynamics 102, 115-120.

Davis, S. D. and C. Frohlich (1991). Single-link cluster analysis, synthetic earthquake catalogues, and aftershock identification. Geophysical Journal International 104 (2), 289-306.

De Guidi, G., R. Caputo, and S. Scudero (2013). Regional and local stress field orientation inferred from quantitative analyses of extension joints: case study from southern Italy. Tectonics 32 (2), 239-251.

De Guidi, G., S. Scudero, and S. Gresta (2012). New insights into the local crust structure of mt. Etna volcano from seismological and morphotectonic data. Journal of Volcanology and Geothermal Research 223, 83-92.

De Natale, G. and F. Pingue (1991). A variable slip fault model for the 1908 Messina Straits (Italy) earthquake, by inversion of levelling data. Geophysical Journal International 104 (1), 73-84.

Del Ben, A., C. Barnaba, and A. Taboga (2008). Strike-slip systems as the main tectonic features in the plio-quaternary kinematics of the Calabrian arc. Marine Geophysical Researches 29 (1), 1-12.

Diggle, P. J. (2013). Statistical Analysis of Spatial and Spatio-Temporal Point Patterns. CRC Press.

El-Isa, Z. and D. Eaton (2014). Spatio-temporal variations in the b-value of earthquake magnitude-frequency distributions: Classification and causes. Tectonophysics 615, 1-11.

Everitt, B., S. Landau, M. Leese, and D. Stahl (2011). Cluster Analysis (Wiley Series in Probability and Statistics). Chichester, UK: Wiley.

Frohlich, C. and S. D. Davis (1990). Single-link cluster analysis as a method to evaluate spatial and temporal properties of earthquake catalogues. Geophysical Journal International 100 (1), 19-32.

Gallais, F., D. Graindorge, M.-A. Gutscher, and D. Klaeschen (2013). Propagation of a lithospheric tear fault (STEP) through the western boundary of the Calabrian accretionary wedge offshore eastern Sicily (Southern Italy). Tectonophysics 602, 141-152.

Galli, P. and V. Bosi (2002). Paleoseismology along the Cittanova fault: implications for seismotectonics and earthquake recurrence in Calabria (southern Italy). Journal of Geophysical Research: Solid Earth 107 (B3), ETG 1-1-ETG 1-19.

Galli, P. A. and E. Peronace (2015). Low slip rates and multimillennial return times for mw 7 earthquake faults in southern Calabria (Italy). Geophysical Research Letters 42 (13), 5258-5265.

Gan, G., C. Ma, and J. Wu (2011). Data clustering: theory, algorithms, and applications. Cambridge: Cambridge 383 University Press.

Gardner, J. and L. Knopoff (1974). Is the sequence of earthquakes in Southern California, with aftershocks

removed, Poissonian?

Bulletin of the Seismological Society of America 64 (5), 1363-1367.

Geyer, C. J. (1999). Likelihood inference for spatial point processes. Stochastic Geometry: Likelihood and Computation 80, 79-140.

Giunta, G., D. Luzio, F. Agosta, M. Calÿ, F. Di Trapani, A. Giorgianni, E. Oliveri, S. Orioli, M. Perniciaro, M. Vitale, et al. (2009). An integrated approach to investigate the seismotectonics of northern Sicily and southern Tyrrhenian. Tectonophysics 476 (1), 13-21.

Guidoboni, E., G. Ferrari, D. Mariotti, A. Comastri, G. Tarabusi, and G. Valensise (2007). Catalogue of strong earthquakes in Italy (461 bc-1997) and Mediterranean Area (760 bc-1500). INGV-SGA (2007) http://storing.ingv.it/cfti4med .

Gutscher, M.-A., S. Dominguez, B. M. Lepinay, L. Pinheiro, F. Gallais, N. Babonneau, A. Cattaneo, Y. Le Faou, G. Barreca, A. Micallef, et al. (2016). Tectonic expression of an active slab tear from high-resolution seismic and bathymetric data offshore Sicily (Ionian Sea). Tectonics 35 (1), 39-54.

Gutscher, M.A., J. Roger, M.-A. Baptista, J. Miranda, and S. Tinti (2006). Source of the 1693 Catania earthquake and tsunami (southern Italy): New evidence from tsunami modeling of a locked subduction fault plane. Geophysical Research Letters 33 (8), L08309.

Hawkes, A. and L. Adamopoulos (1973). Cluster models for earthquakes-regional comparison. Bulletin of the International Statistical Institute 45 (3), 454-461.

Hollenstein, C., H.-G. Kahle, A. Geiger, S. Jenny, S. Goes, and D. Giardini (2003). New GPS constraints on the Africa-Eurasia plate boundary zone in southern Italy. Geophysical Research Letters 30 (18).

Illian, J., A. Penttinen, H. Stoyan, and D. Stoyan (2008). Statistical Analysis and Modelling of Spatial Point Patterns, Volume 70. John Wiley & Sons.

Jacques, E., C. Monaco, P. Tapponnier, L. Tortorici, and T. Winter (2001). Faulting and earthquake triggering during the 1783 Calabria seismic sequence. Geophysical Journal International 147 (3), 499-516.

Jensen, J. L., J. Moller, et al. (1991). Pseudolikelihood for exponential family models of spatial point processes. The Annals of Applied Probability 1 (3), 445-461.

Lavecchia, G., F. Ferrarini, R. de Nardis, F. Visini, and M. S. Barbano (2007). Active thrusting as a possible seismogenic source in Sicily (southern Italy): Some insights from integrated structural-kinematic and seismological data. Tectonophysics 445 (3), 145-167.

Locati, M., R. Camassi, and M. Stucchi (2011). Data base macrosismico Italiano.

Martorana, R., P. Capizzi, G. Avellone, A. D'Alessandro, R. Siragusa, and D. Luzio (2016). Assessment of a geological model by surface wave analyses. Journal of Geophysics and Engineering 14 (1), 159.

Mignan, A. and J. Woessner (2012). Estimating the magnitude of completeness for earthquake catalogs, community online resource for statistical seismicity analysis, doi: 10.5078/corssa-00180805.

Molchan, G. and O. Dmitrieva (1992). Aftershock identification: methods and new approaches. Geophysical Journal International 109 (3), 501-516.

Møller, J. and R. P. Waagepetersen (2003). Statistical Inference and Simulation for Spatial Point Processes. Boca Raton: Chapman and Hall/CRC.

Monaco, C., P. Tapponnier, L. Tortorici, and P. Gillot (1997). Late quaternary slip rates on the Acireale-Piedimonte normal faults and tectonic origin of Mt. Etna (Sicily). Earth and Planetary Science Letters 147 (1-4), 125-139.

Montone, P., M. T. Mariucci, and S. Pierdominici (2012). The Italian present-day stress map. Geophysical Journal International 189 (2), 705-716.

Musumeci, C., L. Scarfò, M. Palano, and D. Patanè (2014). Foreland segmentation along an active convergent margin: New constraints in South-eastern Sicily (Italy) from seismic and geodetic observations. Tectonophysics 630, 137-149.

Neri, G., G. Barberi, G. Oliva, and B. Orecchio (2004). Tectonic stress and seismogenic faulting in the area of the 1908 Messina earthquake, south Italy. Geophysical research letters 31 (10).

Neri, G., G. Barberi, G. Oliva, and B. Orecchio (2005). Spatial variations of seismogenic stress orientations in Sicily, south Italy. Physics of the Earth and Planetary Interiors 148 (2), 175-191.

Neri, G., A. Marotta, B. Orecchio, D. Presti, C. Totaro, R. Barzaghi, and A. Borghi (2012). How lithospheric subduction changes along the Calabrian Arc in southern Italy: geophysical evidences. International Journal of Earth Sciences 101 (7), 1949-1969.

Neri, G., G. Oliva, B. Orecchio, and D. Presti (2006). A possible seismic gap within a highly seismogenic belt crossing Calabria and eastern Sicily, Italy. Bulletin of the Seismological Society of America 96 (4A), 1321-1331.

Ogata, Y. (1988). Statistical models for earthquake occurrences and residual analysis for point processes. Journal of the American Statistical Association 83 (401), 9-27.

Orecchio, B., D. Presti, C. Totaro, and G. Neri (2014). What earthquakes say concerning residual subduction and STEP dynamics in the Calabrian Arc region, south Italy. Geophysical Journal International 199

(3), 1929-1942.

Palano, M. (2015). On the present-day crustal stress, strain-rate fields and mantle anisotropy pattern of Italy. Geophysical Journal International 200 (2), 967-983.

Palano, M., L. Ferranti, C. Monaco, M. Mattia, M. Aloisi, V. Bruno, F. Cannavÿ, and G. Siligato (2012). GPS velocity and strain fields in Sicily and southern Calabria, Italy: updated geodetic constraints on tectonic block interaction in the central Mediterranean. Journal of Geophysical Research: Solid Earth 117 (B7).

Palano, M., D. Schiavone, M. Loddo, M. Neri, D. Presti, R. Quarto, C. Totaro, and G. Neri (2015). Active upper crust deformation pattern along the southern edge of the Tyrrhenian subduction zone (NE Sicily): Insights from a multidisciplinary approach. Tectonophysics 657, 205-218.

Pierdominici, S. and O. Heidbach (2012). Stress field of Italy-mean stress orientation at different depths and wave-length of the stress pattern. Tectonophysics 532, 301-311.

Pino, N. A., D. Giardini, and E. Boschi (2000). The December 28, 1908, Messina Straits, southern Italy, earthquake: Waveform modeling of regional seismograms. Journal of Geophysical Research: Solid Earth 105 (B11), 25473-25492.

Pino, N. A., A. Piatanesi, G. Valensise, and E. Boschi (2009). The 28 December 1908 Messina Straits earthquake (mw 7.1): A great earthquake throughout a century of seismology. Seismological Research Letters 80 (2), 243-259.

Polonia, A., L. Torelli, L. Gasperini, and P. Mussoni (2012). Active faults and historical earthquakes in the Messina Straits area (Ionian Sea). Natural Hazards and Earth System Sciences 12 (7), 2311.

Polonia, A., L. Torelli, P. Mussoni, L. Gasperini, A. Artoni, and D. Klaeschen (2011). The Calabrian arc subduction complex in the Ionian Sea: Regional architecture, active deformation, and seismic hazard. Tectonics 30 (5), TC5018.

Presti, D., A. Billi, B. Orecchio, C. Totaro, C. Faccenna, and G. Neri (2013). Earthquake focal mechanisms, seismogenic stress, and seismotectonics of the Calabrian Arc, Italy. Tectonophysics 602, 153-175.

R Development Core Team (2005). R: A language and environment for statistical computing. Vienna, Austria: R Foundation for Statistical Computing. ISBN 3-900051-07-0.

Reasenberg, P. (1985). Second-order moment of central California seismicity, 1969-1982. Journal of Geophysical Research: Solid Earth 90 (B7), 5479-5495.

Ripley, B. D. (1976). The second-order analysis of stationary point processes. Journal of Applied Probability 13, 255-266.

Ripley, B. D. (1988). Statistical Inference for Spatial Processes. Cambridge University Press.

Rovida, A., M. Locati, R. Camassi, B. Lolli, and P. Gasperini (2016). Cpti15, the 2015 version of the parametric catalogue of Italian earthquakes. istituto nazionale di geofisica e vulcanologia.

Scarfò, L., G. Barberi, C. Musumeci, and D. Patanè (2016). Seismotectonics of northeastern Sicily and southern Calabria (Italy): New constraints on the tectonic structures featuring in a crucial sector for the central Mediterranean geodynamics. Tectonics 35 (3), 812-830.

Scarfò, L., A. Messina, and C. Cassisi (2013). Sicily and southern Calabria focal mechanism database: a valuable tool for local and regional stress-field determination. Annals of Geophysics 56 (1), D0109.

Schick, R. (1977). Eine seismotektonische Bearbeitung des Erdbebens von Messina im Jahre 1908 [neunzehnhundertacht]. Ph. D. thesis, Bundesanstalt für Geowiss. u. Rohstoffe.

Selvaggi, G. and C. Chiarabba (1995). Seismicity and p-wave velocity image of the southern Tyrrhenian subduction zone. Geophysical Journal International 121 (3), 818-826.

Serpelloni, E., R. B*f*rgmann, M. Anzidei, P. Baldi, B. M. Ventura, and E. Boschi (2010). Strain accumulation across the Messina Straits and kinematics of Sicily and Calabria from GPS data and dislocation modeling. Earth and Planetary Science Letters 298 (3), 347-360.

Serpelloni, E., G. Vannucci, S. Pondrelli, A. Argnani, G. Casula, M. Anzidei, P. Baldi, and P. Gasperini (2007). Kinematics of the Western Africa-Eurasia plate boundary from focal mechanisms and GPS data.

Siino, M., G. Adelfio, J. Mateu, M. Chiodi, and A. D'Alessandro (2017). Spatial pattern analysis using hybrid models: an application to the Hellenic seismicity. Stochastic Environmental Research and Risk Assessment 31 (7), 1633-1648.

Silverman, B. W. (1986). Density Estimation for Statistics and Data Analysis, Volume 26. London: Chapman and Hall/CRC.

Sulli, A., V. L. Presti, M. G. Morticelli, and F. Antonioli (2013). Vertical movements in NE Sicily and its offshore: Outcome of tectonic uplift during the last 125 ky. Quaternary International 288, 168-182.

Tinti, S., A. Maramai, and L. Graziani (2004). The new catalogue of Italian tsunamis. Natural Hazards 33 (3), 439-465.

Tortorici, L., C. Monaco, C. Tansi, and O. Cocina (1995).

Recent and active tectonics in the Calabrian arc (Southern Italy). Tectonophysics 243 (1), 37-55.

Uhrhammer, R. (1986). Characteristics of northern and central California seismicity. Earthquake Notes 57 (1), 21.

Valensise, G., R. Basili, and P. Burrato (2008). La sorgente del terremoto del 1908 nel quadro sismotettonico dello Stretto di Messina. In Il Terremoto e il Maremoto del 28 dicembre 1908-Analisi sismologica, impatto, prospettive. Dipartimento della Protezione Civile, Istituto Nazionale di Geofisica e Vulcanologia.

Valensise, G. and D. Pantosti (1992). A 125 kyr-long geological record of seismic source repeatability: the Messina Straits (Southern Italy) and the 1908 earthquake (ms 7/2). Terra Nova 4 (4), 472-483.

Van Stiphout, T., J. Zhuang, and D. Marsan (2012). Seismicity declustering. community online resource for statistical seismicity analysis. doi: 10.5078/corssa-52382934.

*CORRESPONDING AUTHOR: Giada ADELFIO,
Dipartimento di Scienze Economiche , Aziendali e Statistiche,
Università degli Studi di Palermo, Palermo, Italy
email: giada.adelfio@unipa.it